



Delft University of Technology

A study of in-situ sediment flocculation in the turbidity maxima of the Yangtze Estuary

Guo, Chao; He, Qing; Guo, Leicheng; Winterwerp, Johan C.

DOI

[10.1016/j.ecss.2017.04.001](https://doi.org/10.1016/j.ecss.2017.04.001)

Publication date

2017

Document Version

Accepted author manuscript

Published in

Estuarine, Coastal and Shelf Science

Citation (APA)

Guo, C., He, Q., Guo, L., & Winterwerp, J. C. (2017). A study of in-situ sediment flocculation in the turbidity maxima of the Yangtze Estuary. *Estuarine, Coastal and Shelf Science*, 191, 1-9.
<https://doi.org/10.1016/j.ecss.2017.04.001>

Important note

To cite this publication, please use the final published version (if applicable).
Please check the document version above.

Copyright

Other than for strictly personal use, it is not permitted to download, forward or distribute the text or part of it, without the consent of the author(s) and/or copyright holder(s), unless the work is under an open content license such as Creative Commons.

Takedown policy

Please contact us and provide details if you believe this document breaches copyrights.
We will remove access to the work immediately and investigate your claim.

1 **A study of in-situ sediment flocculation in the turbidity maxima of**
2 **the Yangtze Estuary**

3

4 Chao Guo^a, Qing He^{a,*}, Leicheng Guo^a, Johan C. Winterwerp^b

5

6 ^a State Key Laboratory of Estuarine and Coastal Research, East China Normal
7 University, Shanghai 200062, People's Republic of China

8 ^b Section of Environmental Fluid Mechanics, Faculty of Civil Engineering and
9 Geosciences, Delft University of Technology, PO Box 5048, 2600 GA Delft, The
10 Netherlands

11

12

13

14

15 Corresponding author: Qing He

16 Email address: qinghe@sklec.ecnu.edu.cn

17 Phone number: +86 (021) 6223 3688

18 Postal address: State Key Laboratory of Estuarine and Coastal Research, East China
19 Normal University, Shanghai 200062, People's Republic of China

20

21

22

23

24

25

26

27

28

29

30 Highlights:

- 31 1. In-situ floc properties are examined in the turbidity maxima of the Yangtze
32 Estuary.
- 33 2. Flocculation exhibits strong temporal and vertical variations over a tidal cycle.
- 34 3. Turbulence exerts major control on flocculation in this case.
- 35 4. Tidally varying flocculation has implication on siltation in the estuarine turbidity
36 maxima.

37

38

39

40

41

42

43

44

45

46

47

48

49

50

51

52

53

54

55

56

57

58

59

60 **Abstract**

61 In order to improve our understandings of temporal and vertical variations of
62 sediment flocculation dynamics within the turbidity maxima (TM) of the highly turbid
63 Yangtze Estuary (YE), we deployed LISST-100C, a laser instrument for in-situ
64 monitor of the sizes and concentrations of flocculated particles in a wet season. Field
65 data in terms of vertical profiles of flow velocity, suspended sediment concentration
66 (SSC), salinity, flocculated particle size distribution and volume concentration were
67 obtained, based on field works conducted at consecutive spring, moderate, and neap
68 tides.

69 Data analyses show that the mean floc diameters (D_M) were in the range of 14-95
70 μm , and flocculation exhibited strong temporal and vertical variations within a tidal
71 cycle and between spring-neap cycles. Larger D_M were observed during high and low
72 slack waters, and the averaged floc size at neap tide was found 57% larger than at
73 spring tide. Effective density of flocs decreased with the increase of floc size, and
74 fractal dimension of flocs in the YE was mainly between 1.5 and 2.1. We also
75 estimated the settling velocity of flocs by 0.04-0.6 mm s^{-1} and the largest settling
76 velocity occurred also at slack waters. Moreover, it is found that turbulence plays a
77 dominant role in the flocculation process. Floc size decreases significantly when the
78 shear rate parameter G is $>2-3 \text{ s}^{-1}$, suggesting the turbulence breaking force.
79 Combined effects of fine sediment flocculation, enhanced settling process, and high
80 sediment concentration resulted in a large settling flux around high water, which can
81 in part explain the severe siltation in the TM of the YE, thus shedding lights on the
82 navigation channel management.

83 **Keywords:** Sediment flocculation; Floc settling; Turbidity maxima; the Yangtze
84 Estuary.

85

86

87

88

89

90 **1. Introduction**

91 Flocculation plays an important role in cohesive sediment transport, which has been
92 observed in various natural aquatic environments, including fresh and saline waters
93 (Eisma, 1986; Droppo and Ongley, 1992; Dyer and Manning, 1999). Transportation of
94 fine-grained suspended sediment is heavily dependent on the formation of flocs and
95 their enhanced settling velocities which are orders of magnitude larger than that of the
96 primary particles (Dyer, 1989; Whitehouse et al., 2000; Manning, 2004; Mehta, 2013).
97 Therefore modelling and predicting cohesive sediment behavior demand good
98 understandings of flocculation and floc settling processes (Soulsby et al., 2013). Since
99 flocs are dynamic during transportation and they are highly fragile, traditional water
100 sampling method may disrupt the flocs and unable to get the real properties of flocs in
101 field. Hence in-situ instruments and techniques were needed and well developed, e.g.,
102 photography and video system (Eisma et al., 1990; Fennessy et al., 1994a; Manning
103 and Dyer, 1999), and in-situ laser diffraction particle sizers (Agrawal and Pottsmith,
104 2000; Mikkelsen and Pejrup, 2001). The LISST (Laser In-Situ Scattering and
105 Transmissiometry) is such an in-situ instrument widely used for flocculation studies
106 (Mikkelsen and Pejrup, 2001; Fugate and Friedrichs, 2002; Xia et al., 2004; Curran et
107 al., 2007; Guo and He, 2011; Markussen and Andersen, 2014). It is user-friendly and
108 easy to handle in obtaining floc size distributions and volume concentrations.
109 Moreover, LISST can be used to collect flocs information at different water depths
110 and in a broader space scale, much easier and more quickly and cost efficient than
111 using of cameras.

112 Brownian motion, differential settling, and fluid shears are three fundamental
113 factors causing collision and aggregation of primary particles (Tsai et al., 1987).
114 Many researches in the early periods had concluded that effects of Brownian motion
115 on flocculation in estuarine and coastal environments were negligible (McCave, 1984;
116 Partheniades, 1993; van Leussen, 1994). And the effect of differential settling was
117 found much small through experiments by Stolzenbach and Elimelech (1994).
118 Therefore, a number of researches focused on the effects of turbulent shears, turbidity,
119 salinity, and biochemical processes on the development of flocs (Droppo and Ongley,

120 1992; Milligan and Hill, 1998; Winterwerp, 1998; Dyer and Manning, 1999; van
121 Leussen, 1999). Fennessy et al. (1994b) reported that high current shears exert
122 controlling influence on flocculation processes based on field data and Mietta et al.
123 (2009) suggested that mean floc size increases with increasing organic matter content
124 based on laboratory examinations and so on. van der Lee (2000) found that an
125 increase in floc size with increasing suspended sediment concentration (SSC) in the
126 Dollard Estuary, which disagrees with the results of Burban et al. (1989). Dyer (1989)
127 provided a classical conceptual diagram on variations of floc size with SSC and
128 turbulent shear, which showed that low shear promotes floc growth due to collision
129 whereas a high shear leads to floc break-up, and the floc size increases with
130 increasing SSC in quiescent water, however, larger flocs formed at higher
131 concentrations are easily disrupted by shears. The conceptual model was confirmed
132 by some works but did not meet all the situations and most of the researches were
133 conducted in the low turbidity environments with SSC smaller than about 0.5 g l^{-1}
134 (Milligan and Hill, 1998; Manning and Dyer, 1999; Xia et al., 2004; Markussen and
135 Andersen, 2014; Sahin, 2014). It thus still needs more work in highly turbid systems
136 to further extend our understandings of flocculation dynamics.

137 This study is devoted to examining flocculation in the estuarine turbidity maxima
138 (TM) of the Yangtze Estuary (YE), a river- and tide-controlled muddy system with
139 high SSC. Based on the laboratory and field researches, it was found that floc size
140 increased with increase of SSC below 10 g l^{-1} , and the optimum salinity range for
141 flocculation was 4-15‰ and the critical current velocity for flocculation was about
142 $40\text{-}50 \text{ cm s}^{-1}$ in the YE (Zhang et al., 1995; Guan et al., 1996; Jiang et al., 2002; Tang,
143 2007; Wan et al., 2015). But most of the existed researches in the YE were from lab
144 experiments, and less research had been focused on the variation of flocculation
145 through water column in spring-neap tidal cycles.

146 Training works in the North Passage (NP) of the YE in the aim to achieve a 12.5 m
147 deep-water navigation channel lead to a huge amount of dredging requirement
148 (60-100 million m^3 every year) (Xie et al., 2010; Song and Wang, 2013). It is thus
149 eagerly to know where the sediments come from and how the sediments deposit in the

150 NP. Since the NP locates in the estuarine TM zone of the YE which is characterized
151 by high SSC of fine sediment, understandings of flocculation processes and their
152 impacts on sediment transport will benefit searching for answers of why siltation is
153 such high in the NP. We aim to get a better understanding of flocculation dynamics in
154 the estuary, and the purposes of this study are to reveal floc properties at different
155 tidal phases in the TM of the YE, and identify its implications on the channel siltation
156 from the point view of flocculation.

157

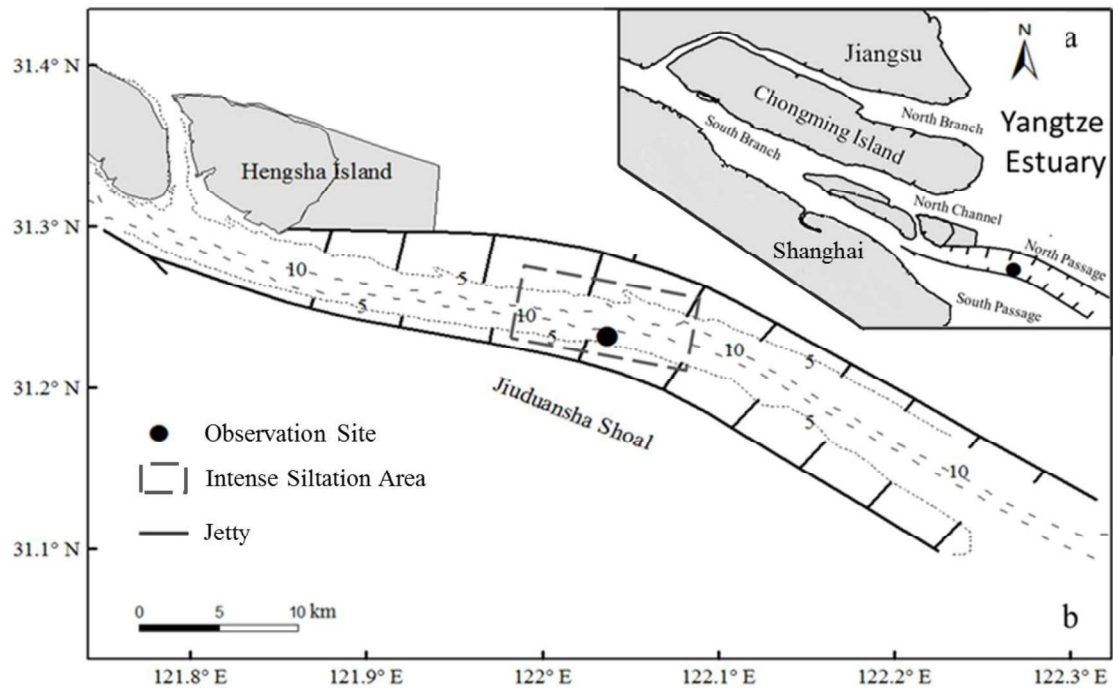
158 **2. Field work and methodology**

159 **2.1. Introduction to the Yangtze Estuary**

160 The YE is a meso-tidal estuary with a mean tidal range of 2.66 m and spring tidal
161 range up to 5 m. The annual river flow is approximately 9,000 km³ (1950-2010) at
162 Datong, a station about 640 km landward the estuary mouth, and the water discharge
163 at Datong is usually used to represent discharge to the YE. The mean and maximal
164 water discharges in 2014 are about 28,000 m³ s⁻¹ and 56,300 m³ s⁻¹, respectively. And
165 the decadal maximal discharge at Datong is 65,100 m³ s⁻¹ (2005-2014). The
166 morphology of the YE is featured by three bifurcations and four outlets (see Figure
167 1a). The NP is now a man-made 12.5 m (below reference level) deep-water
168 navigational channel. The NP is 92.2 km long and the observation site located in the
169 middle part of this channel, where most back-silting occurred in recent years (Figure
170 1b).

171 The tide is irregularly semi-diurnal and the mean ebb tide duration is approximately
172 7.5 hours. Water depth is about 13 m (below mean water level) at the observation site
173 and peak ebb and flood current velocities are 2.8 m s⁻¹ and 1.8 m s⁻¹ at spring tide, and
174 peak ebb and flood velocities are 1.6 m s⁻¹ and 1.2 m s⁻¹, respectively, at neap tide.
175 The median diameters of suspended primary particles are mainly about 6-9 μm, and
176 constitutes of particles include about 40% clay, 54% silt, and 6% sand in this area.

177



178
 179 Fig. 1. Map of the morphology of the Yangtze estuary and the field observation site
 180 (black circle dot). Bathymetric contours of 5 and 10 shown are in meters referenced to
 181 the lowest low water.

182

183 2.2. In-situ measurements

184 Field works were conducted between July 13 and July 23 (wet season) in 2014,
 185 including spring, moderate, and neap tidal conditions. River discharges are about
 186 $46,000 \text{ m}^3 \text{ s}^{-1}$ at Datong during the field survey. A shipboard downward-looking
 187 ADCP (Acoustic Doppler Current Profilers) was used to measure current velocity.
 188 The sampling interval was 10 s and the bin size was 0.5 m. In-situ flocculated particle
 189 size distributions were measured with the LISST-100 (type C), and the range of
 190 particle size that the LISST-100C can differentiate is 2.5-500 μm with an accuracy of
 191 1 phi. The LISST is based on light transmittance through a sample volume of water, it
 192 emits and records the laser in 32 scattering angle ranges, and then the signal is
 193 inverted to a volume distribution over 32 rings (Agrawal and Pottsmith, 2000). The
 194 LISST was lowered through the water column at a steady speed from 0.5 m below
 195 surface to 1 m above the bottom at a depth interval of about one-fifth of water depth
 196 every hour. LISST was set to sample every 5 seconds, and it measured at each layer

197 (totally 6 layers) for at least 1 minute. A volume 1.2 liters of water sample was also
198 collected every hour at 7 different water depths (0, 0.2, 0.4, 0.6, 0.8, 0.9 and 1.0 water
199 depth) with an alpha water sampler, which was used for analyzing salinity, SSC, and
200 primary particle size distribution.

201 Primary particle sizes were analyzed by a Coulter Counter after removing organic
202 material and destroying flocs with sonification. By removing organic materials with
203 hydrogen peroxide in lab, information of primary particles of both the macroflocs and
204 microflocs could be obtained (Van Leussen, 1999). SSC were determined by filtration
205 through pre-weighed filters, then the filters were dried at 60°C for eight hours. The
206 organic matter contents of the sediment collected in spring and neap tide were
207 determined through ignition at 450°C for 6 hours, results showed that organic matter
208 in the mud of YE was about 3% ($\pm 1\%$).

209

210 **2.3. Data processing**

211 *Floc properties*

212 The LISST-100C recorded in-situ particle size distributions every 5 seconds, and
213 then the raw data were analyzed by the LISST-SOP (version 5.00). The processed data
214 were averaged over 1 min in each layer in order to eliminate short-term variations
215 (Mikkelsen and Pejrup, 2001). The mean floc diameter D_M was calculated from the
216 volume concentration distribution, and mean effective density of floc $\Delta\rho$ was
217 calculated as below (Fettweis, 2008):

$$218 \quad \Delta\rho = \rho_F - \rho_W = \frac{M_P}{V_F} - \rho_W = \left(1 - \frac{\rho_W}{\rho_P}\right) \frac{M_P}{V_F} \quad (1)$$

219 where ρ_F is floc density, ρ_W is water density, V_F is the floc volume concentration
220 derived from LISST and M_P indicates the mass suspended sediment concentration
221 measured through filtration of water samples. ρ_P is primary particle density which is
222 estimated to be 2,570 kg m⁻³, given a density of 1,300 kg m⁻³ for organic matter
223 (Markussen and Andersen, 2013) and an organic matter content of 3% (mass ratio)
224 determined by loss on ignition. The effective densities of flocs are used here to
225 indicate the ability of the flocs being suspended in the water in counteracting the

226 buoyancy.

227 Based on the self-similar fractal entities, it was proposed by Kranenburg (1994)
228 that:

$$229 \quad \Delta\rho \propto (\rho_P - \rho_W) \left(\frac{D_M}{d}\right)^{nf-3} \quad (2)$$

230 where d is the diameter of the primary particle and nf is the floc fractal dimension, a
231 mathematical parameter used as an indicator of particle morphology. The fractal
232 dimension of flocs usually varies between about 1.4 for large fragile flocs, and about
233 2.2 for strong flocs (Kranenburg, 1994).

234 During this investigation, all the mean floc diameters were smaller than 100 μm ,
235 thus the Stokes' formula was used to estimate settling velocity as follows:

$$236 \quad \omega_s = \frac{D_M^2 \Delta\rho g}{18\mu} \quad (3)$$

237 where g is the acceleration due to gravity and μ is the molecular viscosity of water.

238 *Turbulent shear*

239 The shear rate parameter G in the logarithmic velocity layer was calculated in
240 accordance with Pejrup and Mikkelsen (2010):

$$241 \quad G = \sqrt{\frac{u_*^3 (1-z/H)}{\nu \kappa z}} \quad (4)$$

242 where ν is the kinematic viscosity, κ is Von Karman's constant ($\kappa=0.41$), z is the height
243 above bed, H is the water depth and u_* is the friction velocity, it can be calculated
244 through:

$$245 \quad u_* = \frac{u_b \kappa}{\ln(z/z_0)} \quad (5)$$

246 u_b is the current velocity, z_0 is the roughness length, and z_0 is assumed to be constant
247 of 3 mm in this work. This value has been used in the simulation of sediment
248 transport in the turbidity maxima of the YE (Ge et al., 2012).

249

250 **3. Results**

251 **3.1. Hydrodynamics and sediment concentrations**

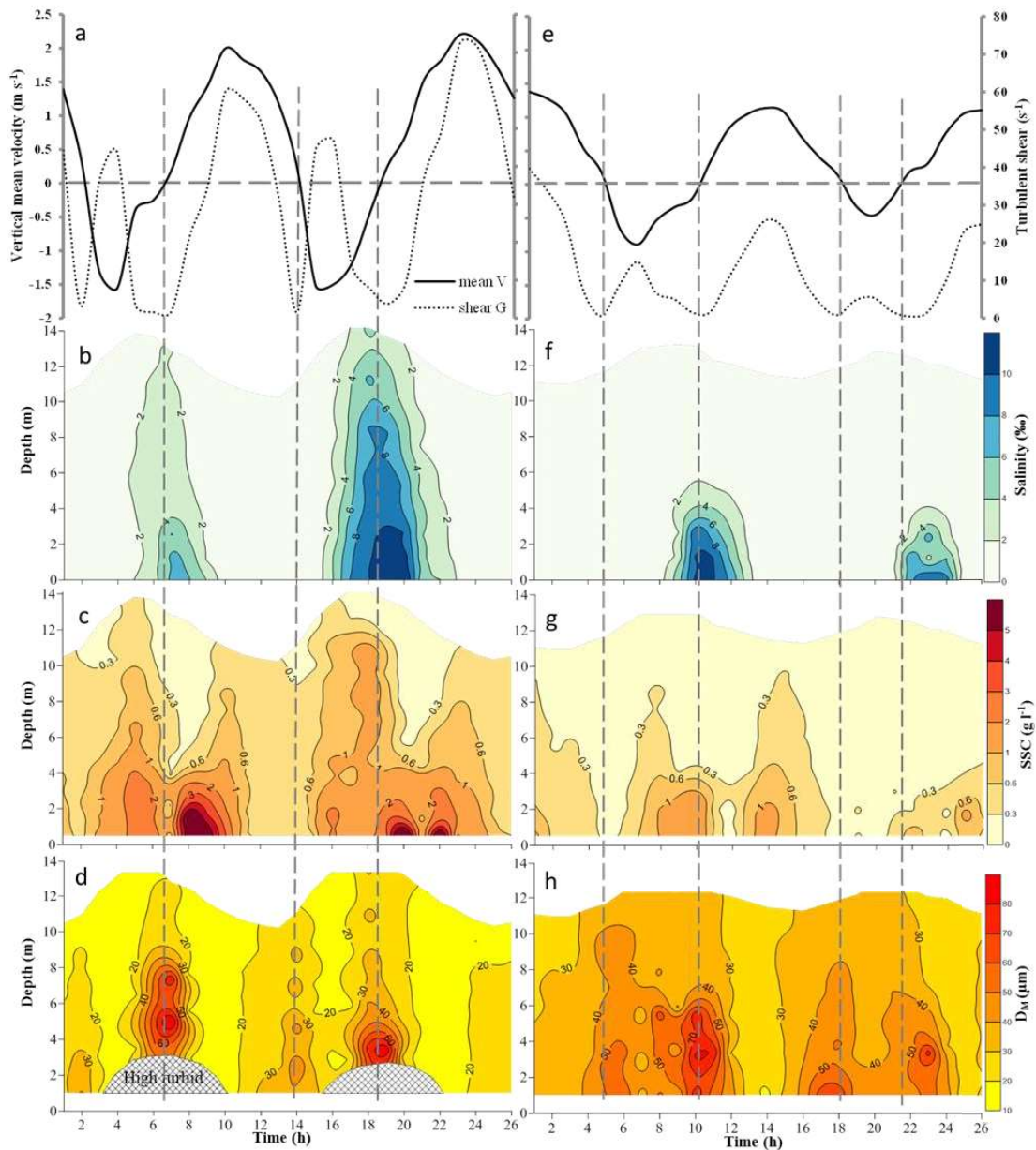
252 Figure 2 shows vertically and time varying mean flow velocity, near bottom
253 turbulence, salinity, SSC, and mean floc size at spring and neap tides.

254 During the field survey period, there were no strong winds, so the influence of wind

255 and wind-generated waves can be ignored. Turbulent shear in the water was mainly
256 caused by flow velocity and varied with tidal phases.

257 The time series of current velocities suggested that tidal waves were asymmetrical
258 with an ebb-dominance, the maximum vertically-averaged ebb flow velocities were
259 2.3 m s^{-1} and 1.4 m s^{-1} at spring and neap tides, respectively (Figures 2a, and 2e).
260 During flood period, acceleration and deceleration stages were also asymmetrical. It
261 only took about 2 hours from low water slack (LWS) to maximum flood, which was
262 one half of the decelerating time. However, the time of accelerating and decelerating
263 during ebb was almost the same.

264 Vertical variations of salinity and SSC over time are presented also in Figure 2.
265 Salinity was lower than 2‰ most of the time, and the maximum salinity was about 11‰
266 at both spring and neap tides. Large salinity only lasted a few hours around high water
267 slack (HWS). At spring tide, the smallest SSC through the water column was about
268 0.1 g l^{-1} and SSC was larger than 0.3 g l^{-1} most of the time. The mean SSC was
269 $0.68 \pm 0.28 \text{ g l}^{-1}$ and there were four peaks of SSC during the investigation period of
270 two tidal cycles. Increased current velocity led to high near-bed turbulent shears and
271 resulted in sediment resuspension around the peak flood periods. During the shift
272 from flood to ebb, the near bottom SSC increased fast, and the largest SSC reached 7
273 g l^{-1} . High SSC in the surface of water column dropped rapidly around HWS which
274 can be attributed to flocculation-enhanced settling. At neap tide, SSC became smaller
275 compared to spring tide. The maximum bottom SSC was 1.73 g l^{-1} and the averaged
276 SSC over the whole tidal cycle was $0.24 \pm 0.12 \text{ g l}^{-1}$. Overall SSC increased with
277 increased bottom shear stress.



278

279 Fig. 2. (a, e) Vertical mean flow velocity and turbulent shear (ebb is positive), (b, f)
 280 salinity in ‰, (c, g) suspended sediment concentration in g l^{-1} , and (d, h) distribution
 281 of mean floc size in μm . Left panels are results at spring tide, and right four panels are
 282 the results at neap tide.

283

284 3.2. Floc parameters

285 *Mean floc diameter*

286 The D_M varied between 14 and 95 μm in a tidal cycle at spring tide with a mean
 287 value of $27 \pm 13 \mu\text{m}$ (Figure 2d). The mean D_M was $43 \pm 10 \mu\text{m}$ at neap tide, about 57%
 288 larger than spring tide. Floc sizes varied largely in a tidal cycle. Larger flocs

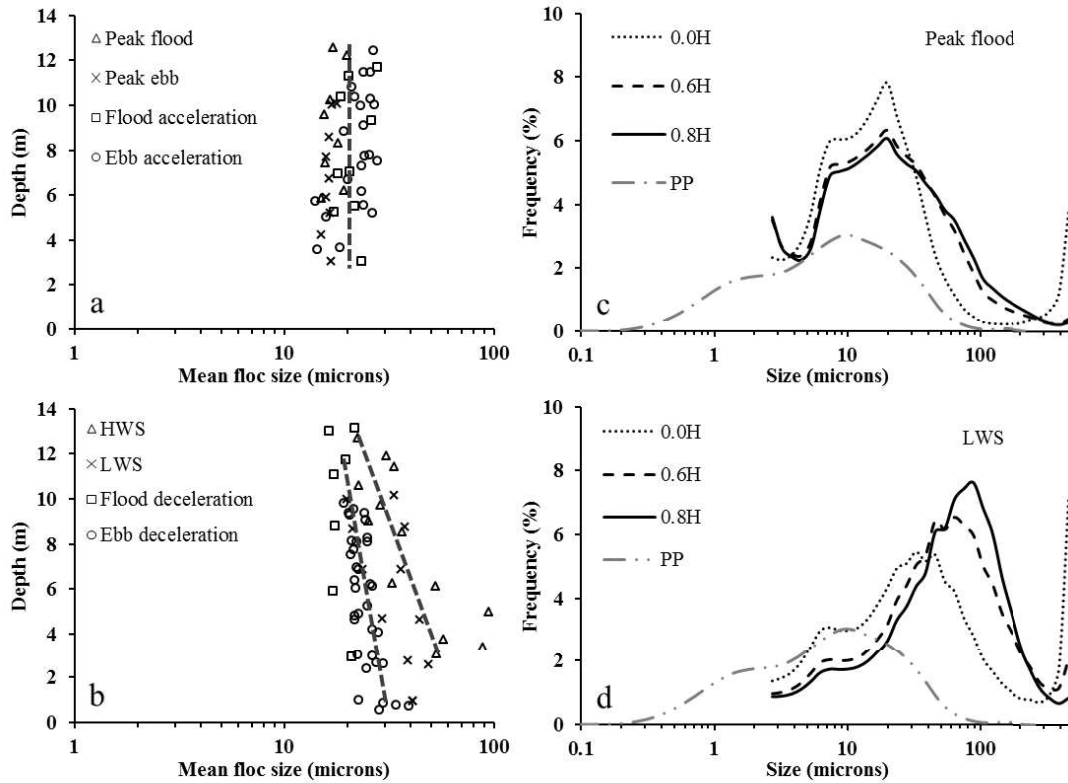
289 developed around slack waters of low turbulent intensity, and flocs were larger during
290 HWS than LWS. It was found that the largest flocs systematically occurred with the
291 peaks of salinity around HWS. Floc size increased from surface to near bottom during
292 slack water, though, part of the near bottom data were not obtained as a result of too
293 high turbidity for LISST to work normally. Smaller flocs persisted at time with strong
294 turbulence, particularly around peak flood and ebb tides.

295

296 *Vertical distribution and particle size distribution (PSD)*

297 Figures 3a, and 3b show vertical profiles of mean floc sizes during different typical
298 tidal phases at spring tide. Flocs were smallest in size when current magnitudes were
299 maximal and flocs at different depths were larger during the slack water period. D_M
300 was uniform at all depths at both flood and ebb acceleration and peak velocity periods.
301 However, D_M increased from surface layer to near bottom layer during the time of
302 deceleration and slack waters, which can be ascribed to differential settling when the
303 turbulent shear was low.

304 Figures 3c and 3d show PSDs of in-situ flocs at peak flood and LWS and the
305 averaged PSD of primary particles. The PSD of primary particles is unimodal with a
306 peak at about 10 μm , but that of in-situ flocs detected by LISST are mainly bimodal.
307 One peak of the floc PSD corresponds to 10 μm as the PSD of primary particles,
308 whereas the second peak of floc PSD around 30-90 μm is more prominent. The larger
309 peak at LWS increased from surface to bottom layers, the same tendency as D_M
310 profile. Note that there were raised tails at both ends of the distribution curves,
311 because of the presence of flocs beyond the confined measurement range (2.5-500
312 μm) of LISST. These flocs with diameter $<2.5 \mu\text{m}$ and $>500 \mu\text{m}$ are likely to cause
313 over- or under-estimation of D_M to some degree, respectively. Voulgaris and Meyers
314 (2004) tried to minimize this effect by creating additional rings corresponding to
315 larger size bands, and it turned out that this measure did not cause a big difference
316 because the dominant portion of flocs are detected by LISST. For that reason, the
317 impact of the tails on the PSD of flocs was not treated.



318

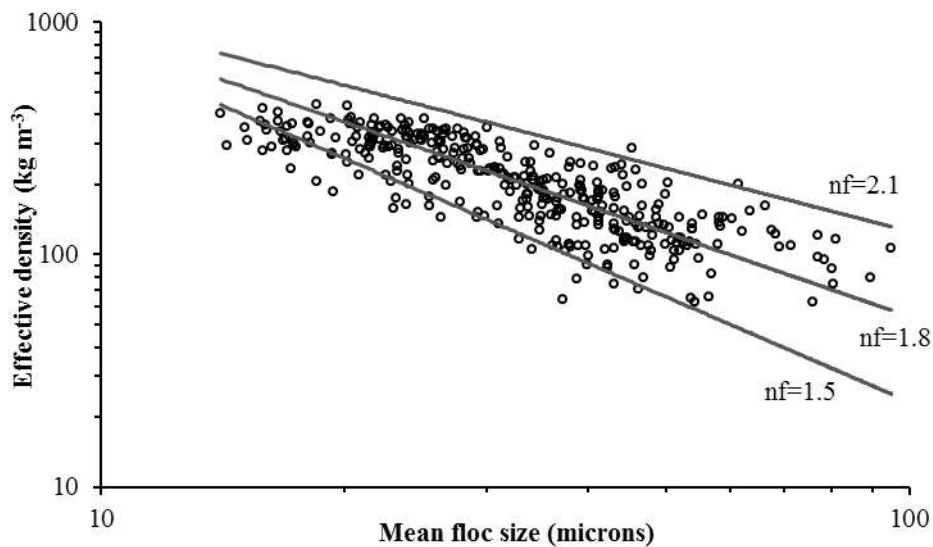
319 Fig. 3. Panels (a) and (b) show vertical variations of mean floc size in different tidal
 320 phases, and panels (c) and (d) show size distributions of both dispersed and
 321 flocculated particles. Panel (c) shows the results at peak flood and (d) shows the
 322 results at LWS at spring tide. PP indicates primary particle, and H is the water depth.

323

324 *Effective density and settling velocity of flocs*

325 The effective density of flocs calculated by equation (1) varied between 60 and 450
 326 kg m^{-3} . It tended to decrease with increasing floc size and the mean effective density
 327 of all the flocs observed was 215 kg m^{-3} (Figure 4). However, there was a wide
 328 scattering of effective density for a certain D_M . Most of the floc size was in the range
 329 of $30\text{-}60 \mu\text{m}$, and the largest spread of effective density also occurred in this range,
 330 indicating that the effective densities of flocs with the same D_M might change
 331 significantly due to various floc structures. The fractal dimension nf was estimated to
 332 be in the range of $1.5\text{-}2.1$, and the best fit is $nf=1.8$ in this field survey (see Figure 4).
 333 An fractal dimension of 1.8 was smaller than the average $nf=2$ concluded by
 334 Winterwerp (1998) through published researches in the Ems Estuary, the North Sea

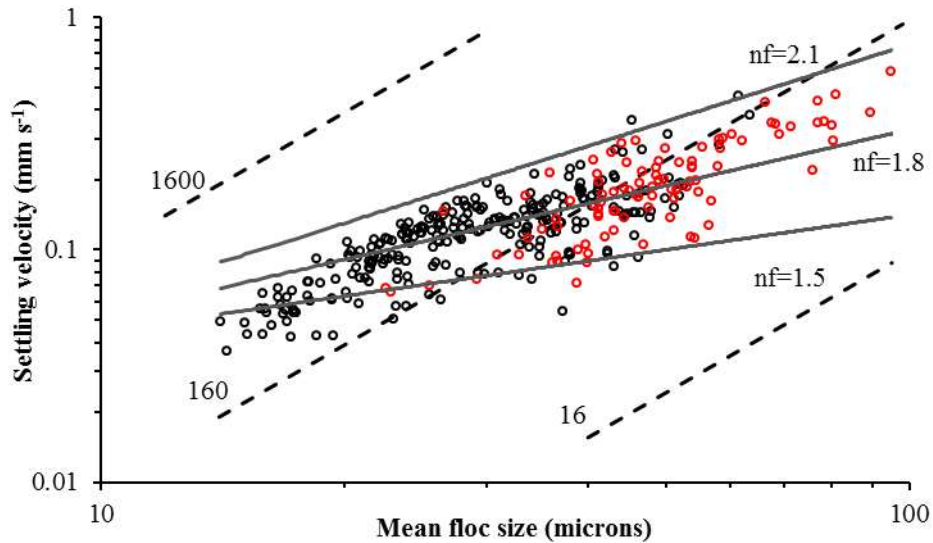
335 (van Leussen, 1994), and the Tamar Estuary (Fennessy et al., 1994a), indicating that
336 flocs in the YE might be more fragile.



337

338 Fig. 4. Variations of effective density with mean floc size.

339 Settling velocities of flocs varied between 0.04 and 0.6 mm s⁻¹ in this study, and it
340 increased with increasing D_M (see Figure 5). Most of the settling velocities were in
341 the range of 0.08-0.3 mm s⁻¹. Note that the same floc size group might have settling
342 velocities varying in a big range, and on the other hand flocs of varying sizes may
343 have the same settling velocity due to the difference in floc structure and density. It
344 was found that most of the large settling velocities occurred at water slack periods,
345 which were marked as red circles in Figure 5. The averaged settling velocity at water
346 slack periods was 0.2 mm s⁻¹, which was 67% larger than the averaged result of 0.12
347 mm s⁻¹ in the other time. Shi et al. (2003) calculated settling velocities of 0.4-4.1 mm
348 s⁻¹ based on Rouse SSC profiles in the YE. But vertical SSC profiles have many kinds
349 of patterns as a result of the complex hydrodynamics in estuaries, thus the Rouse SSC
350 profile is not representative in a tidal system. The research of Shao et al. (2010)
351 showed that high sediment concentrations caused by resuspension will mislead to
352 greater settling velocity through Rouse equation, and this may be the reason that the
353 smallest and largest settling velocity calculated by Shi et al. (2003) was much larger
354 than the estimation in this study (0.04 mm s⁻¹ and 0.6 mm s⁻¹, respectively).



355

356 Fig. 5. Variations of settling velocities of flocs with D_M . Red and black circles were
 357 results at water slack periods and other time, respectively. Dashed lines of 1,600, 160
 358 and 16 represent the effective density isolines of spherical quartz particles, the unit is
 359 kg m^{-3} , and grey lines show the relationships of settling speed and size under different
 360 floc fractal dimensions.

361

362 4. Discussion

363 4.1. Flocculation processes

364 It is known that transportation of suspended cohesive sediment is mainly driven by
 365 the cycle of suspension, flocculation, settling, deposition, erosion, and resuspension
 366 (Eisma, 2012). Flocculation process plays a key role in this cycle as it can affect the
 367 size and density of suspended particles, and control the settling velocity of sediment.
 368 Meanwhile, heavy metal, contaminants, and pollutants can easily adhere to flocs,
 369 thus the fate and transport of flocs could also have great effects in biochemical matter
 370 transport.

371 Large flocs or macroflocs ($>125 \mu\text{m}$, Eisma, 1986) have a larger diameter and
 372 smaller density, and potentially larger settling velocity, thus tend to account for most
 373 of the vertical settling flux (Fennessy et al., 1997; Manning and Dyer, 2007). On the
 374 other hand, the large flocs are more fragile, less denser and can be easily broken down
 375 into smaller ones. On the contrary, smaller flocs or microflocs ($<125 \mu\text{m}$) usually have

376 a denser structure, higher density, and are more resilient to turbulent breaking force,
377 and they have a high potential to aggregate again to form larger flocs (Dyer and
378 Manning, 1999).

379 Data collected in this field survey revealed flocculation dynamic variations within a tidal
380 cycle and the spring-neap cycle. The variances of mean flocculation size through the water
381 column shown in Figures 2d and 2h indicated active flocculation and break-up
382 processes in the YE. The D_M ranged between 14-95 μm and 20-80 μm during spring
383 tide and neap tide, respectively. However, the variations of primary particle size were
384 much more limited, with median size around 6-8 μm . Meanwhile, the bimodal PSDs
385 of flocs (see Figures 3c and 3d) with a small peak at around 10 μm similar to that of
386 primary particles indicated that a part of inert particles are still disaggregated in the
387 natural environments, and other parts of primary populations flocculated and formed a
388 more significant larger peak, varying from 30 to 90 μm .

389 Within a tidal cycle, it was found that large flocs occurred systematically around
390 slack water at both spring and neap tides, and the averaged flocculation size around water
391 slack was 45 ± 20 μm at spring tide. However, it was only 22 ± 5 μm at other tidal
392 phases. Between spring-neap tidal cycles, although the maximal flocculation size observed at
393 spring tide was a little larger, the averaged flocculation size during neap tidal cycles was 57%
394 larger.

395 During slack waters, it was interesting to find that flocs tended to develop from
396 surface to bottom (Figure 3b), suggesting that differential settling could dominate the
397 flocculation process during these low shear stress periods (Chen et al., 1994; Fugate
398 and Friedrichs, 2003). Laboratory experiments with sediment samples of a mud
399 content of 70% by Wendling et al. (2015) exhibited that settling velocity at the bottom
400 of the settling column was 20 times larger than that at surface, also indicating
401 significant flocculation occurred during settling in still water.

402

403 **4.2. Controls on in-situ flocculation**

404 *Effects of Turbulent Shear*

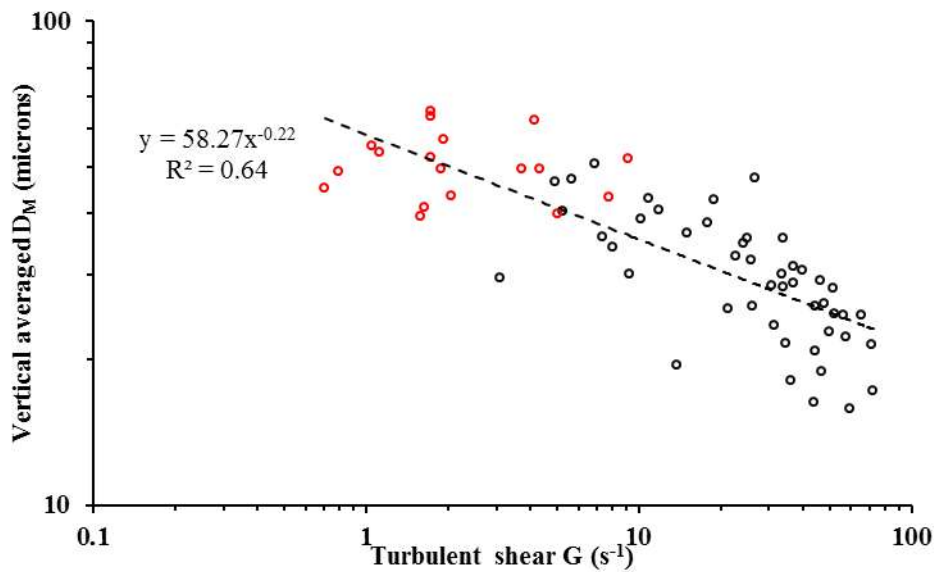
405 Among many influential factors, turbulence is thought to be the controlling factor

406 determining maximum floc sizes in tidal cycles (Winterwerp, 1998; Dyer and
407 Manning, 1999). It is also widely known that there is a critical shear stress beneficial
408 to flocculation mostly. Below this threshold, an increase in turbulence strength would
409 increase the collision frequency of particles, thus leading to stronger aggregation.
410 Increase of turbulence strength beyond the threshold would break up fragile flocs
411 (Eisma, 1986; Manning and Dyer, 1999; Winterwerp, 2002), and resulting in floc
412 disruption. The critical shear stress was found in many published works, including
413 laboratory experiments by Manning and Dyer (1999) and field study by Sahin (2014)
414 and Markussen and Andersen (2014), and in their researches, a critical shear value of
415 0.35 N m^{-2} ($G \approx 27 \text{ s}^{-1}$), $G \approx 20 \text{ s}^{-1}$, and G of about 4 s^{-1} was obtained, respectively,
416 suggesting a big range of variations.

417 In this study, Figure 6 shows the relationship between D_M and turbulent dissipation
418 parameter G . The regression of our field data did not quantify critical shear well, and
419 an overall negative relationship between D_M and G was got, with the regression
420 parameter $R^2=0.64$. A plateau of floc size for G values $<3 \text{ s}^{-1}$ was identified, and when
421 turbulent shear became larger than 3 s^{-1} , D_M decreased significantly with the
422 increasing G , once turbulent shear G exceeded $40\text{-}50 \text{ s}^{-1}$, D_M through water column
423 were only about $20 \mu\text{m}$, suggesting that almost all flocs excepted the strongest small
424 ones broke up under high turbulent shear.

425 The largest vertically-averaged D_M of flocs is about $70 \mu\text{m}$ in the present work,
426 which is much smaller than many other field observations conducted in less turbid
427 estuaries (Eisma and Li, 1993; Curran et al., 2007; Wang et al., 2013). As we know,
428 floc size is the result of dynamic equilibrium between flocculation and break-up
429 processes, and biological factors could mediate both processes. On one hand, the
430 organic material can adhere to primary particles, change their surface charge, and
431 increase the probability of cohesion after collision (Mietta et al., 2009). On the other
432 hand, Winterwerp and van Kesteren (2004) showed that many organic matters contain
433 long polymers, which might connect different particles through ‘bridging’. Thus the
434 increasing of organic matter could increase turbulent shear threshold in breaking flocs.
435 In this study, low content of organic matter about 3% in the high turbid YE might

436 contribute to the overall small flocs compared to other systems.



437

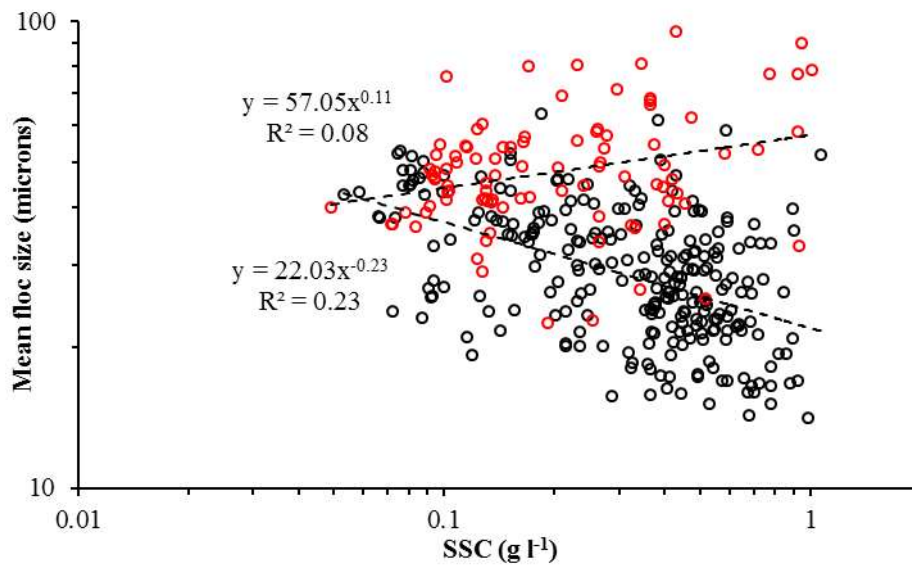
438 Fig. 6. Variations of vertical averaged D_M with turbulent shear. Red and black circles
439 are results at water slack periods and other time, respectively.

440

441 *Impacts of SSC*

442 Increasing SSC within a range will lead to increased particle collision frequency
443 and enhance floc growth (Eisma and Li, 1993; van der Lee, 2000). However, the
444 effects of SSC on flocculation were found insignificant in some lab and field work
445 (Milligan and Hill, 1998; Xia et al., 2004). Moreover, Burban et al. (1989) found that
446 median floc size decreased as the SSC increased in their experiments. Note that these
447 observations were confined to environments with SSC around $0.05-0.25 \text{ g l}^{-1}$, which
448 was smaller than the typical turbidity range in this study, i.e., $0.05-1.1 \text{ g l}^{-1}$. A wide
449 scatter of D_M corresponds to SSC was shown in Figure 7. Floc size tended to increase
450 with increasing SSC at water slack periods and a negative relationship was found in
451 other tidal periods. However, it is noticed that both the correlations are poor ($R^2=0.23$
452 and $R^2=0.08$, respectively). We think that the highly variable estuarine environments
453 might lead to the opposite tendency and poor correlations between floc size and SSC.
454 As flocculation is influenced by both physical and biochemical processes, and many
455 factors that have effects on the processes can be dependent on each other and change
456 simultaneously (e.g., turbulence, SSC, salinity, and organic matter). Moreover, SSC is

457 related to the resuspension process, which plays an important role in determining near
458 bottom floc size distributions (Fugate and Friedrichs, 2003).



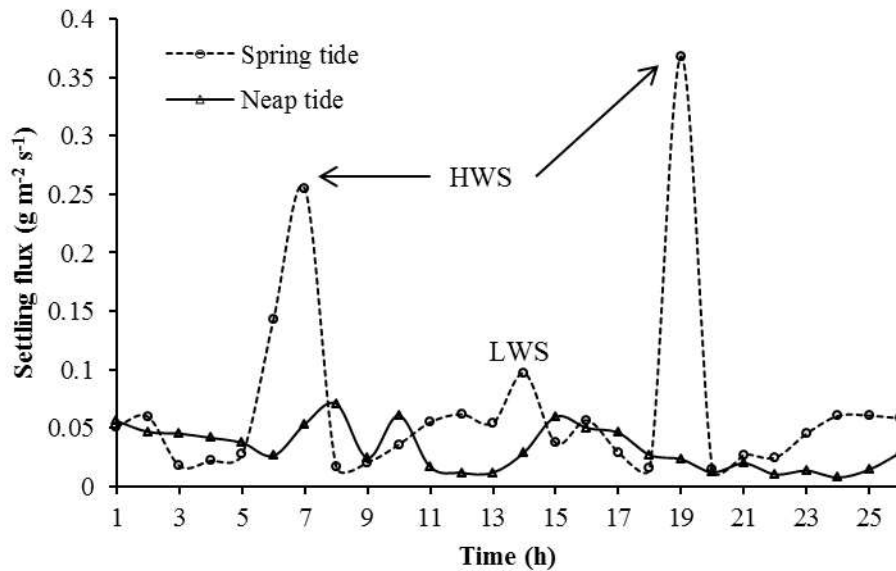
459
460 Fig. 7. Variations of mean floc size with SSC. Red and black circles are results at
461 water slack periods and other time, respectively.

462

463 4.3. Implications for siltation

464 Floc settling velocity and SSC both varied significantly in a tidal cycle. The largest
465 settling velocity occurred around HWS in the NP, and it was found that SSC
466 decreased sharply after HWS at spring tide (see Figure 2c). The rapid decreasing of
467 SSC was mainly caused by fast settling of large flocs that developed during low
468 turbulence intensity. We estimated vertical settling flux by multiplying SSC and
469 settling velocity of flocs. At neap tide, the time varying settling flux ranged between
470 0.01-0.07 g m⁻² s⁻¹, and the averaged settling flux was 0.032 g m⁻² s⁻¹ (Figure 8). The
471 averaged value at spring tide was 0.066 g m⁻² s⁻¹, and the settling fluxes at HWS and
472 LWS at spring tide were about 0.3 and 0.1 g m⁻² s⁻¹, respectively, which was a few
473 times larger than the settling fluxes in the other periods. The fast settling speed of
474 large flocs especially around HSW together with high SSC through water column
475 resulted in huge settling flux around high water. Uncles et al. (2010) observed similar
476 phenomenon in the Tamar Estuary that a rapid reduction of SSC on flood tides within
477 2.5 h of HW. Moreover, the upward flux around HW was small, indicating that the

478 settling of large flocs around HW played a controlling role in the deposition of
 479 suspended sediment. And after the fast settling of particles at HWS, large amounts of
 480 sediment are confined predominantly within the bottom layer, thus they will not be
 481 easily transported seaward in the following ebb period. These would lead to rapid
 482 accumulation of sediment in the study area.



483

484 Fig. 8. Time varying settling fluxes of sediment at spring and neap tides.

485

486 5. Conclusions

487 This study examined in-situ flocculation dynamics based on data of current and
 488 sediment properties in the TM of the YE. Floc diameter was measured by a
 489 LISST-100C, and settling velocity was estimated based on floc size and effective
 490 density.

491 Mean floc diameters varied between 14-95 μm and flocculation exhibited strong
 492 temporal and vertical variations within a tidal cycle and between spring-neap cycles.
 493 Large flocs occurred systematically around slack waters and floc sizes increased from
 494 surface to bottom during the deceleration and slack water periods. The averaged floc
 495 size at neap tide was 57% larger than at spring tide. Effective density of flocs
 496 decreased with the increase of floc size, and fractal dimension of floc in the YE was
 497 mainly between 1.5 and 2.1.

498 Turbulent shear plays a dominant role in controlling processes of flocs aggregation

499 and break-up. Floc size decreased significantly with the increase of turbulent shear
500 when turbulent shear was beyond the range of 2-3 s⁻¹. Correlations between SSC and
501 floc size was poor suggesting SSC is not significant in controlling flocculation in this
502 study based on the field data.

503 Settling velocity of flocs ranged between 0.04-0.6 mm s⁻¹ and it changed in
504 different tidal phases. The largest settling flux happened at the HWS during spring
505 tide, which was caused by fast settling of large flocs together with high SSC. This
506 mechanism might be an important factor leading to rapid accumulation of sediment at
507 the study area where serious back-siltation happened during the wet season. Future
508 work is needed to examine the flocculation sensitivity to the physical parameters in a
509 more quantified manner with laboratory experiments.

510

511 **Acknowledgements**

512 The study is funded by the National Natural Science Foundation of China (NSFC)
513 (No. 51320105005, 41276080, 41506105) and SKLEC-fund (No. 2015RCDW02).
514 The comments and suggestions from two anonymous reviewers and the associate
515 editor Andrew J. Manning are greatly appreciated.

516

517

518 **References**

- 519 Agrawal, Y.C., Pottsmith, H.C., 2000. Instruments for particle size and settling
520 velocity observations in sediment transport. *Mar. Geol.* 168, 89–114.
521 doi:10.1016/S0025-3227(00)00044-X
- 522 Burban, P.Y., Lick, W., Lick, J., 1989. The flocculation of fine-grained sediments in
523 estuarine waters. *J. Geophys. Res.* 94, 8323–8330.
524 doi:10.1029/JC094iC06p08323
- 525 Chen, S., Eisma, D., Kalf, J., 1994. In situ distribution of suspended matter during the
526 tidal cycle in the elbe estuary. *Netherlands J. Sea Res.* 32, 37–48.
527 doi:10.1016/0077-7579(94)90026-4
- 528 Curran, K.J., Hill, P.S., Milligan, T.G., Mikkelsen, O.A., Law, B.A., Durrieu de
529 Madron, X., Bourrin, F., 2007. Settling velocity, effective density, and mass
530 composition of suspended sediment in a coastal bottom boundary layer, Gulf of
531 Lions, France. *Cont. Shelf Res.* 27, 1408–1421. doi:10.1016/j.csr.2007.01.014
- 532 Droppo, I.G., Ongley, E.D., 1992. The state of suspended sediment in the freshwater
533 fluvial environment: a method of analysis. *Water Res.* 26, 65–72.
- 534 Dyer, K.R., 1989. Sediment processes in estuaries: Future research requirements. *J.*
535 *Geophys. Res.* 94, 14327–14339. doi:10.1029/JC094iC10p14327
- 536 Dyer, K.R., Manning, A.J., 1999. Observation of the size, settling velocity and

537 effective density of flocs, and their fractal dimensions. *J. Sea Res.* 41, 87–95.

538 Eisma, D., 2012. *Suspended matter in the aquatic environment*. Springer Science &
539 Business Media.

540 Eisma, D., 1986. Flocculation and de-flocculation of suspended matter in estuaries.
541 *Netherlands J. Sea Res.* 20, 183–199. doi:10.1016/0077-7579(86)90041-4

542 Eisma, D., Li, A., 1993. Changes in suspended-matter floc size during the tidal cycle
543 in the Dollard estuary. *Netherlands J. Sea Res.* 31, 107–117.

544 Eisma, D., Schuhmacher, T., Boekel, H., Van Heerwaarden, J., Franken, H., Laan, M.,
545 Vaars, A., Eijgenraam, F., Kalf, J., 1990. A camera and image-analysis system
546 for in situ observation of flocs in natural waters. *Netherlands J. Sea Res.* 27,
547 43–56. doi:10.1016/0077-7579(90)90033-D

548 Fennessy, M.J., Dyer, K.R., Huntley, D.A., 1994a. inssev: An instrument to measure
549 the size and settling velocity of flocs in situ. *Mar. Geol.* 117, 107–117.
550 doi:10.1016/0025-3227(94)90009-4

551 Fennessy, M.J., Dyer, K.R., Huntley, D.A., 1994b. Size and settling velocity
552 distributions of flocs in the Tamar Estuary during a tidal cycle. *Aquat. Ecol.* 28,
553 275–282.

554 Fennessy, M.J., Dyer, K.R., Huntley, D.A., Bale, A.J., 1997. Estimation of settling
555 flux spectra in estuaries using INSSEV, in: *Cohesive Sediments—proc. of*
556 *INTERCOH Conf.* Wiley, Chichester. pp. 87–104.

557 Fettweis, M., 2008. Uncertainty of excess density and settling velocity of mud flocs
558 derived from in situ measurements. *Estuar. Coast. Shelf Sci.* 78, 426–436.
559 doi:10.1016/j.ecss.2008.01.007

560 Fugate, D.C., Friedrichs, C.T., 2003. Controls on suspended aggregate size in partially
561 mixed estuaries. *Estuar. Coast. Shelf Sci.* 58, 389–404.
562 doi:10.1016/S0272-7714(03)00107-0

563 Fugate, D.C., Friedrichs, C.T., 2002. Determining concentration and fall velocity of
564 estuarine particle populations using ADV, OBS and LISST. *Cont. Shelf Res.* 22,
565 1867–1886.

566 Ge, J., Chen, C., Qi, J., Ding, P., Beardsley, R.C., 2012. A dike–groyne algorithm in a
567 terrain-following coordinate ocean model (FVCOM): Development, validation
568 and application. *Ocean Model.* 47, 26–40.

569 Guan, X., Chen, Y., Du, X., 1996. Experimental study on mechanism of flocculation
570 in Yangtze Estuary (in Chinese). *J. Hydraul. Eng.* 6, 70–80.

571 Guo, L., He, Q., 2011. Freshwater flocculation of suspended sediments in the Yangtze
572 River, China. *Ocean Dyn.* 61, 371–386.

573 Jiang, G., Yao, Y., Tang, Z., 2002. Analysis of influencing factors on fine sediment
574 flocculation in the Changjiang Estuary (in Chinese). *Acta Oceanol. Sin.* 21,
575 385–394.

576 Kranenburg, C., 1994. The fractal structure of cohesive sediment aggregates. *Estuar.*
577 *Coast. Shelf Sci.* 39, 451–460. doi:10.1016/S0272-7714(06)80002-8

578 Manning, A.J., 2004. Observations of the properties of flocculated cohesive sediment
579 in three western European estuaries. *J. Coast. Res.* 70–81.

580 Manning, A.J., Dyer, K.R., 2007. Mass settling flux of fine sediments in Northern

581 European estuaries: Measurements and predictions. *Mar. Geol.* 245, 107–122.
582 doi:10.1016/j.margeo.2007.07.005

583 Manning, A.J., Dyer, K.R., 1999. A laboratory examination of floc characteristics
584 with regard to turbulent shearing. *Mar. Geol.* 160, 147–170.
585 doi:10.1016/S0025-3227(99)00013-4

586 Markussen, T.N., Andersen, T.J., 2014. Flocculation and floc break-up related to
587 tidally induced turbulent shear in a low-turbidity, microtidal estuary. *J. Sea Res.*
588 89, 1–11.

589 Markussen, T.N., Andersen, T.J., 2013. A simple method for calculating in situ floc
590 settling velocities based on effective density functions. *Mar. Geol.* 344, 10–18.
591 doi:10.1016/j.margeo.2013.07.002

592 McCave, I.N., 1984. Size spectra and aggregation of suspended particles in the deep
593 ocean. *Deep Sea Res. Part A, Oceanogr. Res. Pap.* 31, 329–352.
594 doi:10.1016/0198-0149(84)90088-8

595 Mehta, A.J., 2013. An introduction to hydraulics of fine sediment transport. World
596 Scientific Publishing Co Inc.

597 Mietta, F., Chassagne, C., Manning, A.J., Winterwerp, J.C., 2009. Influence of shear
598 rate, organic matter content, pH and salinity on mud flocculation. *Ocean Dyn.* 59,
599 751–763. doi:10.1007/s10236-009-0231-4

600 Mikkelsen, O., Pejrup, M., 2001. The use of a LISST-100 laser particle sizer for
601 in-situ estimates of floc size, density and settling velocity. *Geo-Marine Lett.* 20,
602 187–195.

603 Milligan, T.G., Hill, P.S., 1998. A laboratory assessment of the relative importance of
604 turbulence, particle composition, and concentration in limiting maximal floc size
605 and settling behaviour. *J. Sea Res.* 39, 227–241.

606 Partheniades, E., 1993. Turbulence, flocculation and cohesive sediment dynamics.
607 *Nearshore Estuar. cohesive sediment Transp.* 40–59.

608 Pejrup, M., Mikkelsen, O.A., 2010. Factors controlling the field settling velocity of
609 cohesive sediment in estuaries. *Estuar. Coast. Shelf Sci.* 87, 177–185.
610 doi:10.1016/j.ecss.2009.09.028

611 Sahin, C., 2014. Investigation of the variability of floc sizes on the Louisiana Shelf
612 using acoustic estimates of cohesive sediment properties. *Mar. Geol.* 353, 55–64.

613 Shao, Y., Yan, Y., Maa, J.P.-Y., 2010. In situ measurements of settling velocity near
614 Baimao shoal in Changjiang estuary. *J. Hydraul. Eng.* 137, 372–380.

615 Shi, Z., Zhou, H.J., Eittreim, S.L., Winterwerp, J.C., 2003. Settling velocities of fine
616 suspended particles in the Changjiang Estuary, China. *J. Asian Earth Sci.* 22,
617 245–251. doi:10.1016/S1367-9120(03)00067-1

618 Song, D., Wang, X.H., 2013. Suspended sediment transport in the Deepwater
619 Navigation Channel, Yangtze River Estuary, China, in the dry season 2009: 2.
620 Numerical simulations. *J. Geophys. Res. Ocean.* 118, 5568–5590.
621 doi:10.1002/jgrc.20411

622 Soulsby, R.L., Manning, A.J., Spearman, J., Whitehouse, R.J.S., 2013. Settling
623 velocity and mass settling flux of flocculated estuarine sediments. *Mar. Geol.*
624 339, 1–12. doi:10.1016/j.margeo.2013.04.006

625 Stolzenbach, K.D., Elimelech, M., 1994. The effect of particle density on collisions
626 between sinking particles: implications for particle aggregation in the ocean.
627 *Deep. Res. Part I* 41, 469–483. doi:10.1016/0967-0637(94)90091-4

628 Tang, J.H., 2007. Characteristics of fine cohesive sediment's flocculation in the
629 Changjiang estuary and its adjacent sea area. Master Degree thesis, East China
630 Norm. Univ. May.

631 Tsai, C.H., Iacobellis, S., Lick, W., 1987. Flocculation of Fine-Grained Lake
632 Sediments Due to a Uniform Shear Stress. *J. Great Lakes Res.* 13, 135–146.
633 doi:10.1016/S0380-1330(87)71637-2

634 Uncles, R.J., Bale, A.J., Stephens, J.A., Frickers, P.E., Harris, C., 2010. Observations
635 of floc sizes in a muddy estuary. *Estuar. Coast. Shelf Sci.* 87, 186–196.

636 van der Lee, W.T.B., 2000. Temporal variation of floc size and settling velocity in the
637 Dollard estuary. *Cont. Shelf Res.* 20, 1495–1511.
638 doi:10.1016/S0278-4343(00)00034-0

639 van Leussen, W., 1994. Estuarine macroflocs and their role in fine-grained sediment
640 transport. Ministry of Transport, Public Works and Water Management, National
641 Institute for Coastal and Marine Management (RIKZ).

642 van Leussen, W., 1999. The variability of settling velocities of suspended fine-grained
643 sediment in the Ems estuary, in: *Journal of Sea Research.* pp. 109–118.
644 doi:10.1016/S1385-1101(98)00046-X

645 Voulgaris, G., Meyers, S.T., 2004. Temporal variability of hydrodynamics, sediment
646 concentration and sediment settling velocity in a tidal creek. *Cont. Shelf Res.* 24,
647 1659–1683. doi:10.1016/j.csr.2004.05.006

648 Wan, Y., Wu, H., Roelvink, D., Gu, F., 2015. Experimental study on fall velocity of
649 fine sediment in the Yangtze Estuary, China. *Ocean Eng.* 103, 180–187.

650 Wang, Y.P., Voulgaris, G., Li, Y., Yang, Y., Gao, J., Chen, J., Gao, S., 2013.
651 Sediment resuspension, flocculation, and settling in a macrotidal estuary. *J.*
652 *Geophys. Res. Ocean.* 118, 5591–5608.

653 Wendling, V., Gratiot, N., Legout, C., Droppo, I.G., Coulaud, C., Mercier, B., 2015.
654 Using an optical settling column to assess suspension characteristics within the
655 free, flocculation, and hindered settling regimes. *J. Soils Sediments* 15,
656 1991–2003.

657 Whitehouse, R.J.S., Soulsby, R.L., Roberts, W., Mitchener, H.J., 2000. Dynamics of
658 estuarine muds: a manual for practical applications., *Dynamics of estuarine muds:*
659 *a manual for practical applications.* Report SR 527.

660 Winterwerp, J.C., 2002. On the flocculation and settling velocity of estuarine mud.
661 *Cont. Shelf Res.* 22, 1339–1360. doi:10.1016/S0278-4343(02)00010-9

662 Winterwerp, J.C., 1998. A simple model for turbulence induced flocculation of
663 cohesive sediment. *J. Hydraul. Res.* 36, 309–326.

664 Winterwerp, J.C., Van Kesteren, W.G.M., 2004. Introduction to the physics of
665 cohesive sediment dynamics in the marine environment. Elsevier.

666 Xia, X.M., Li, Y., Yang, H., Wu, C.Y., Sing, T.H., Pong, H.K., 2004. Observations on
667 the size and settling velocity distributions of suspended sediment in the Pearl
668 River Estuary, China. *Cont. Shelf Res.* 24, 1809–1826.

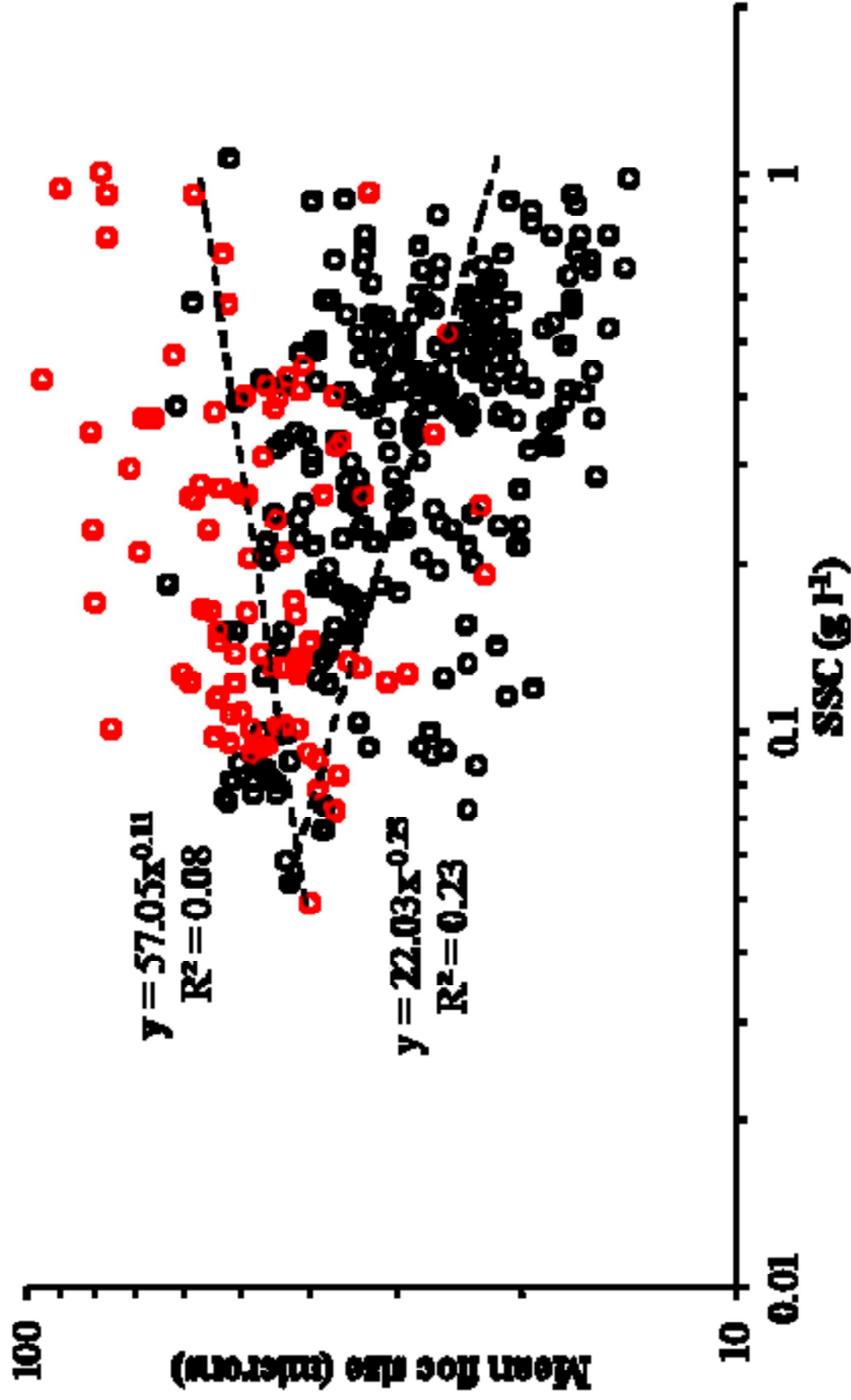
669 doi:10.1016/j.csr.2004.06.009

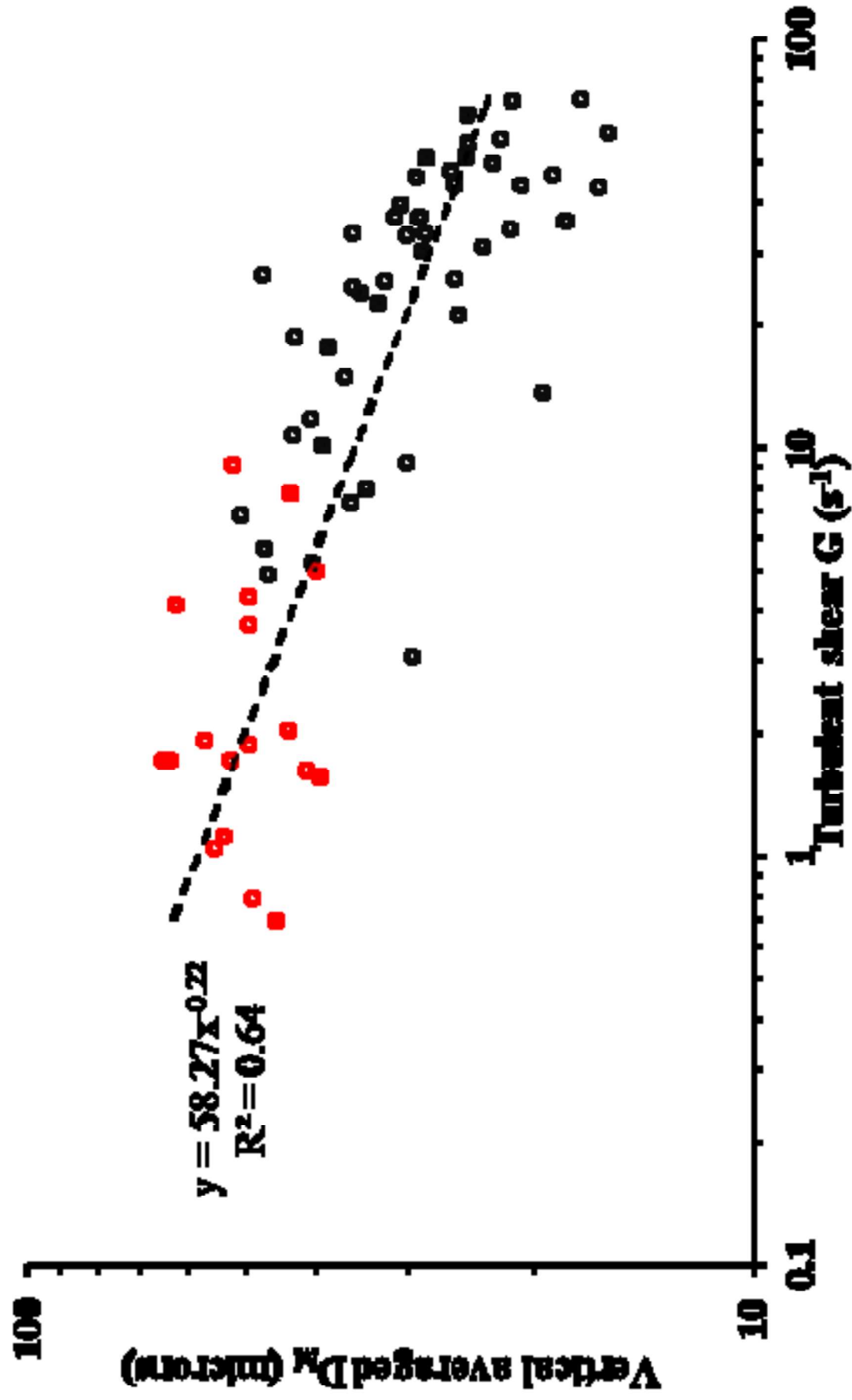
670 Xie, R., Wu, D.A., Yan, Y., Zhou, H., 2010. Fine silt particle pathline of dredging
671 sediment in the Yangtze River deepwater navigation channel based on EFDC
672 model. *J. Hydrodyn. Ser. B* 22, 760–772.

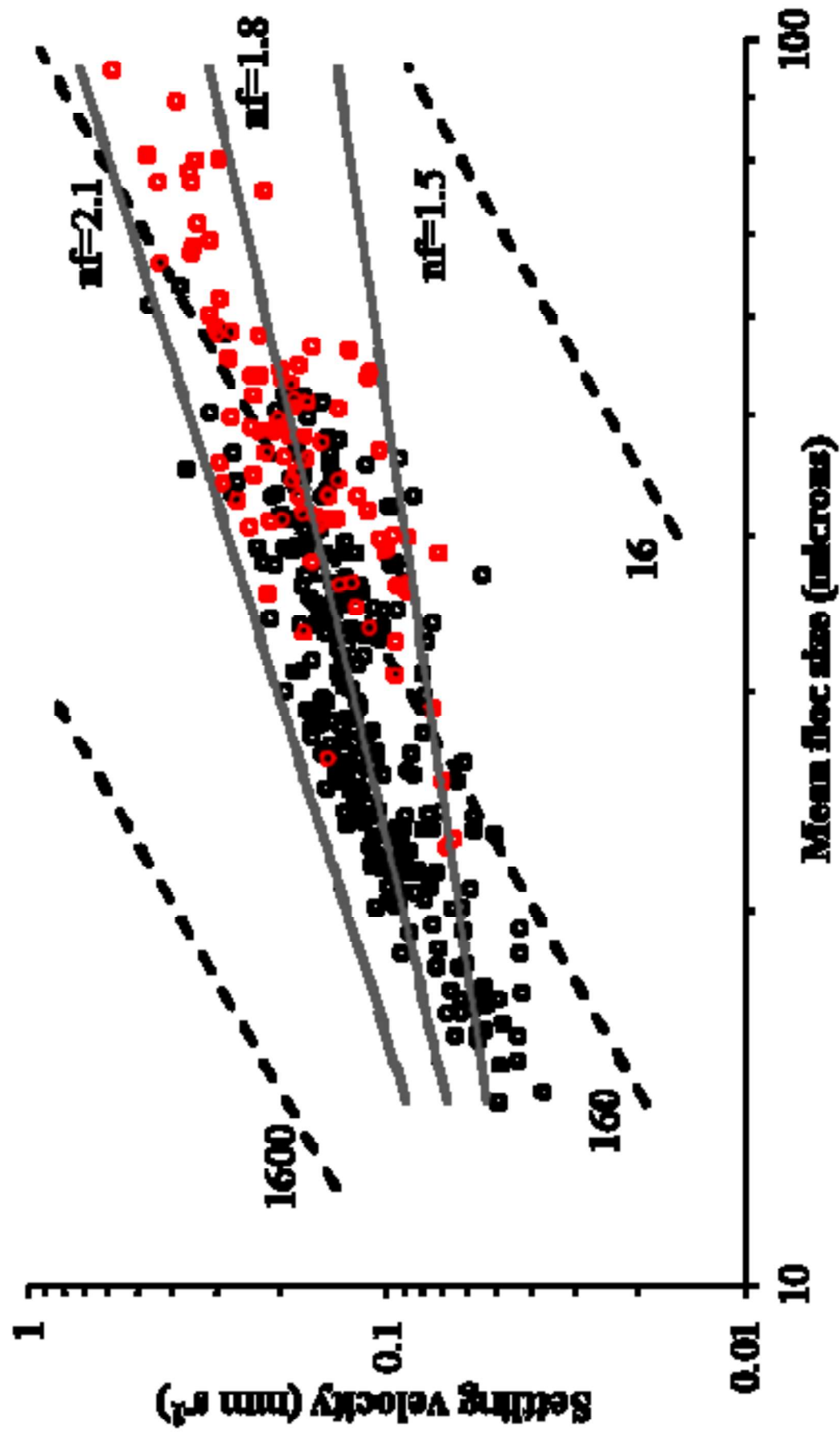
673 Zhang, Z., Ruan, W., Jiang, G., 1995. The relationship between floc settlement in
674 flowing water and deposition in the Changjiang estuary mouth bar area (in
675 Chinese). *Oceanol. Limnol. Sin.* 378–383.

676

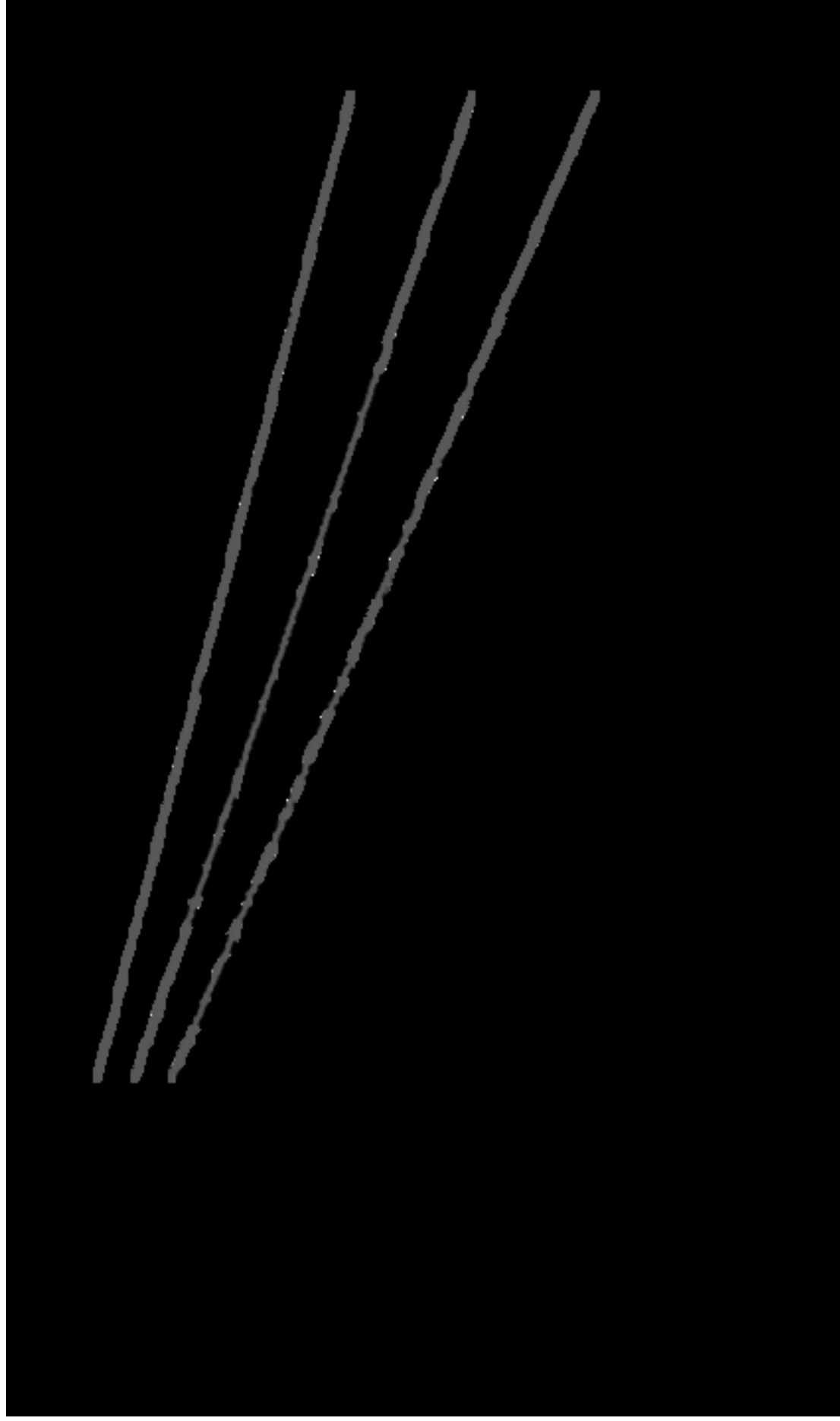








[Click here to download high resolution image](#)





[Click here to download high resolution image](#)

